IEEE Access
Multidisciplinary ⋮ Rapid Review ⋮ Open Access Journal

Received 27 June 2024, accepted 30 July 2024, date of publication 7 August 2024, date of current version 11 September 2024.

Digital Object Identifier 10.1109/ACCESS.2024.3439890

RESEARCH ARTICLE

Model Predictive Control of Variable Refrigerant Flow Systems for Room Temperature Control

CHUN-YEON LIN[1], (Member, IEEE), TING-KUAN LIAO[1], HSIN-HAO CHOU[1], YI-CHIN WU[1], (Member, IEEE), CHIEN-CHANG WANG[2], SHY-HER NIAN[2], MENG-YEN TSAI[2], AND TSAI-WANG HUNG[2]

[1]Department of Mechanical Engineering, National Taiwan University, Taipei 10617, Taiwan
[2]Green Energy and Environment Research Laboratories, Industrial Technology Research Institute, Hsinchu 31040, Taiwan

Corresponding author: Chun-Yeon Lin (chunyeonlin@ntu.edu.tw)

This work was supported by the Energy Administration, Ministry of Economic Affairs, under Grant 112-E0213 and Grant 113-E0213.

ABSTRACT This paper presents a supervisor model-switch method for model predictive control of room temperature using a one-to-three variable refrigerant flow (VRF) system. This method utilizes system identification to obtain linearized transfer functions of the variable refrigerant flow system's compressor speed and electronic expansion valve to room and superheat temperature. The transfer functions for room and the two-phase region temperatures of the evaporator are derived from the energy conservation law to apply in VRF systems. The model predictive control structure is adopted to consider the coupling effects between control states. The effects of superheat and room temperature error weighting factors on rapid cooling and steady-state error are numerically investigated. In addition, this research utilizes a switching linearization model approach to overcome the limitation of a single identification model with a narrow, accurate temperature control range. A supervisor model-switch strategy is proposed to switch multiple models for the same target temperature to average the risk of model mismatch, and calculate the minimum allowable switching time to ensure system stability during switching, thereby expanding the range of temperature control. The proposed method has been experimentally evaluated on a one-to-three VRF system to control the steady-state temperature of each indoor unit within 0.5°C and maintain a superheat above 0°C to avoid liquid refrigerant from entering the compressor.

INDEX TERMS Variable refrigerant flow system, model predictive control, room temperature.

I. INTRODUCTION

The variable refrigerant flow (VRF) system controls the flow rate of refrigerants to different rooms to achieve desired temperatures. Compared to one-to-one air conditioners, VRF systems consist of an outdoor compressor and multiple indoor units to reduce the required compressors and decrease energy consumption in buildings. For central air-conditioning systems, the connected state of air circulation affects each room's air quality. The main issue with VRF systems is their architecture, which connects one outdoor unit to multiple indoor units, causing room temperatures and superheat to interfere with each other and posing a challenge for temperature control. Thus, system modeling is essential for VRF systems to control subsystems and diagnose equipment malfunctions. Such a physical model based on energy, mass, and momentum conservation has been proposed [1]. However, identifying the massive parameters of air conditioning components requires complex processing. System identification is a practical tool for modeling single- or multi-evaporator air-conditioning systems [2], [3], whuch measures system inputs and outputs through data regression to derive the system's state-space equation. Furthermore, a semi-nonlinear ordinary differential heat model has been used to simulate model indoor room temperatures [4].

Various control methods have been applied to refrigeration and airconditioning systems, including on-off control, proportionalintegralderivative (PID) controllers, nonlinear control, robust control, fuzzy logic control, neural network control, and model predictive control (MPC). To improve

The associate editor coordinating the review of this manuscript and approving it for publication was Hassen Ouakad.

the system's transient response, the system can be linearized at a single operating point, and the PID controller parameters can be automatically adjusted using multiobjective particle swarm optimization [5]. Nonlinear control based on linearized feedback, gain scheduling, and nonlinear feedback control can also be applied to control refrigeration and airconditioning systems [6], [7]. However, a one-to-many refrigeration and air-conditioning system involves higher-order system dynamics and, thus, more complex mathematical analysis. In such cases, a multi-input, multi-output robust controller can effectively handle disturbances and uncertainties in system parameters [8] but requires a high-order controller after the model reduction process. Fuzzy control, which bypasses the need for a mathematical model, requires extensive experience and domain knowledge related to refrigeration and air conditioning during the design of fuzzy logic controllers [9], making controller design challenging. Proportional-integral controllers can be combined with neural networks for thermal comfort control [10], ensuring thermal comfort by using the predicted mean vote as the input to train the neural network to adjust occupants' perceived temperature [11]. However, neural network control requires a large amount of training data. VRF systems are slow to respond, making it difficult to obtain sufficient experimental data, thus affecting the development and implementation of control methods.

The MPC design yields high-performance control systems that operate without intervention for periods [12]. MPC has been extensively studied and integrated into heating systems [13]. To optimize a control vector over the prediction horizon, MPC employs a cost function expressed as a tracking error, control effort, demand cost, power consumption, and constraints. These features keep control variables within bounds and improve transient and steady-state responses in VRF systems. The advantages and disadvantages of the MPC method compared with other traditional control methods are listed in Table 1. While MPC requires a physical model as a control reference, for systems with relatively slow response, such as VRF, the process of building a neural network with a large dataset can be time-consuming. PID and Fuzzy control, on the other hand, require a specialized knowledge background for parameter tuning. MPC can mitigate the risk of component damage by considering input-output constraints during the control process using model-based optimization calculations.

According to the arrangements of MPC controllers, the MPC controllers can be categorized as a centralized MPC [14], decentralized MPC, and distributed MPC. The advantages of distributed MPC lie in its controllers being able to exchange data, thereby reducing computational costs and having good output characteristics [15]. Conversely, centralized MPC is characterized by achieving optimal output, but its computational costs are higher than those of the other two forms, making it less suitable for computing cores with limited capabilities. Decentralized MPC has the lowest computational costs among the three forms but produces the least optimal output results. For the cost function parameters in MPC, the Robust MPC combines robust control techniques to overcome model uncertainties [16], [17].

TABLE 1. Controller comparison.

	Physical model	Advantages	Disadvantages
PID	Not necessary	Easy-to-incorporate	Professional knowledge is required to adjust parameters
Neural network	Not necessary	Easy-to-incorporate	Substantial data is required, and its practical application may be challenging in VRF systems.
Fuzzy control	Not necessary	Easy-to-incorporate, and Capable of resisting system uncertainties	Professional knowledge is required to adjust parameters
MPC	Necessary	Physically restricted input and output can be added	It requires establishing a system model and involves high computational complexity.

Furthermore, combining parameter estimation and robust MPC improves control accuracy [18], [19]. The Supervisory MPC involves a hierarchical control architecture, in which a supervisory controller generates setpoints for local controllers. The supervisory controller considers the overall system objectives, such as thermal comfort and temperature regulation, and calculates operating conditions for the system [20], [21]. However, MPC still has some problems that need to be solved, including high computational complexity, difficulty in practical application, and parameter adjustment challenges.

This study applies system identification methods and supervisory centralized MPC as the control strategy in a VRF system. Additionally, it combines a strategy applied in vapor compression systems to achieve zero steady-state errors under unknown thermal loads [22]. For computational costs, this study identifies multiple operating points and expands the controllable range of the system by switching mathematical model controllers. A switching control strategy is proposed to ensure the continuity of signals when switching controllers and to avoid system instability caused by rapid switching by accessing past state values [23]. In the supervisor model-switch strategy, mode dwell time (MDT) is a crucial parameter that ensures the system operates in a stable range before allowing switching [24], [25]. For nonlinear system design, all controllers guarantee Lyapunov decrement and constrain mode switching to ensure the stability of the closed-loop system [26].

This paper aims to investigate temperature control in a one-to-many VRF system. Previous research [1], [27] derived a physical model of a one-to-one air conditioning system. However, most physical models for one-to-many

VRF systems are overly complex, and obtaining their parameters is challenging [28]. Additionally, the two-phase zone temperature of the evaporator cannot be directly measured in experimental setups. Therefore, this paper employs system identification to directly obtain the transfer functions between compressor speed, expansion valve opening, room temperature, and superheat. Through this approach, a linearized model is obtained and used to design the MPC controller. The remainder of this article offers the following.

- The supervisor model-switch method for designing model predictive control of room temperature using a one-to-three VRF system, including model identification, MPC applications, and rules for switching MPC reference models, is introduced.
- The effects of the system identification on VRF systems are numerically investigated using experimental data. The MPC and the supervisor model-switch strategy for the VRF systems are numerically validated.
- The experiments illustrate the feasibility of the MPC and propose a strategy for transitioning models to control the room temperature at the user-set temperature.

II. MODEL PREDICTIVE CONTROL ON VARIABLE REFRIGERANT FLOW SYSTEM

Fig. 1 illustrates a VRF system comprising one outdoor and multiple indoor units to achieve different desired temperatures in each room. In Fig. 1(a), each indoor unit's electronic expansion valve (EEV) controls the flow of liquid refrigerant delivered from the outdoor unit to adjust cooling capacity according to users' desired temperature settings. The gaseous refrigerant flows back to the outdoor unit to release heat from the indoor to the outdoor.

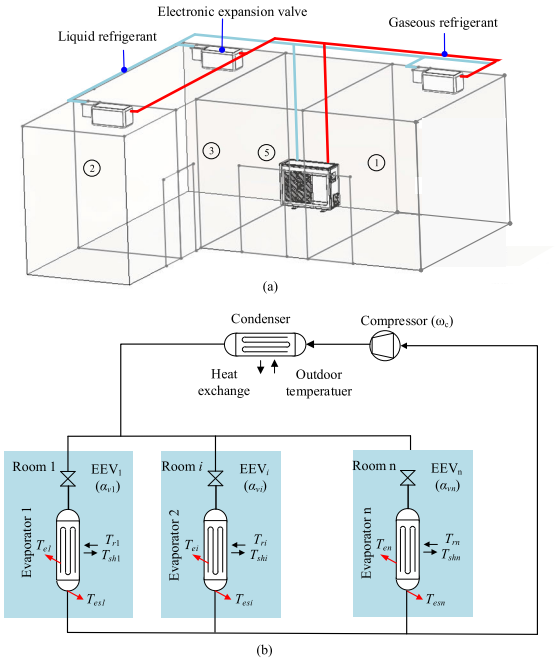

FIGURE 1. Illustration of the working principle of the one-to-many VRF system. (a) Configuration. (b) Physical system architecture.

The configuration of the VRF system, composed of the refrigerant cycle and indoor dynamics, is shown in Fig. 1(b). The compressor compresses the gaseous refrigerant to form a high-temperature and high-pressure refrigerant, which flows into the condenser and exchanges heat with the outdoor environment, resulting in a low-temperature refrigerant.

The EEV distributes the refrigerant into its indoor evaporator to exchange heat with the indoor environment, decreasing the room temperature T_{ri} of rooms i (i= 1, 2, …, n). During the heat exchange process, the refrigerant with liquid and gas coexisting inside the evaporator completely transforms into a gaseous refrigerant with temperature changing from two-phase region temperature (T_{ei}) to evaporator outlet temperature (T_{esi}). The temperature difference between T_{es} and T_e is defined as the superheat temperature T_{sh}, which is greater than 0°C, indicating complete vaporization of the refrigerant. The gaseous refrigerant ultimately flows back to the compressor, completing the refrigerant cycle in the VRF system for cooling. Assuming the fan speeds of the condenser and the indoor air conditioner are constant, the system inputs are the compressor speed (ω_c) and the EEV opening (α_{vi}). The outputs are the room temperature (T_{ri}) and the evaporator's superheat temperature (T_{shi}).

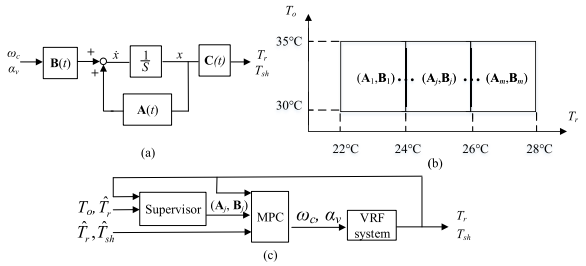

FIGURE 2. Illustration of the supervisor model-switch method for model predictive control of the room temperature. (a) Model of the VRF system. (b) Linearized models. (c) Block diagram of the supervisor model-switch strategy for model predictive control.

The proposed control strategy to control T_r and T_{sh} for the VRF system involves the hardware of the VRF system, supervisor, and MPC, as shown in Fig. 2. As illustrated in Fig. 2(a), the experimental VRF system is modeled as a state-space representation with $\mathbf{A}(t)$, $\mathbf{B}(t)$, and $\mathbf{C}(t)$, which are nonlinear and high-order matrices and can be approximated by the multiple linearized models concerning different equilibrium points. The matrix $\mathbf{C}(t)$ is an identity matrix that outputs the states fully.

Fig. 2(b) shows the VRF model is separated into linearized models ($\mathbf{A}_j$, $\mathbf{B}_j$) (j= 1, 2, …, m), constructed using the system identification method according to the outdoor temperature (T_o) and room temperatures (T_r) within different ranges. When the user sets different room temperatures, an approach is needed to select an appropriate model from the established linear models. Fig. 2(c) shows that the supervisor-controlled layer is added to switch a proper reference model for MPC automatically, which is the supervisory centralized MPC applied in the VRF systems for controlling T_r and T_{sh}.

The user-set room temperature $\hat{T}_r$ and T_o are not only put into the supervisor, but the current room temperature (T_r) and superheat (T_{sh}) are also feedback to switch a model from linearized models ($\mathbf{A}_j$, $\mathbf{B}_j$). The MPC determines each indoor unit's compressor speed and the EEV openings to execute closed-loop control based on the user-set room temperature ($\hat{T}_r$) and superheat temperature ($\hat{T}_{sh}$), reference model, and feedback temperatures. MPC discretizes the system's dynamic equation, uses an iterative algorithm to predict future states to minimize the cost function within a finite time horizon, and calculates the optimal control inputs ω_c and α_v for the next sampling time. The approach reduces model mismatch issues, allowing the system to achieve the user-set temperatures, thereby improving system performance and energy efficiency.

A. DYNAMIC MODEL OF VRF SYSTEMS

In [3], the dynamic model of a triple-evaporator air-conditioning (TEAC) system is given by a system of first-order equations:

$$\begin{bmatrix} \delta T_{e1}(s) \\ \delta T_{sh1}(s) \\ \vdots \\ \delta T_{ei}(s) \\ \delta T_{shi}(s) \\ \vdots \\ \delta T_{en}(s) \\ \delta T_{shn}(s) \end{bmatrix} = \begin{bmatrix} \frac{\tilde{b}_{1,1}}{s+\tilde{a}_1} & \frac{\tilde{b}_{1,2}}{s+\tilde{a}_1} & \cdots & \frac{\tilde{b}_{1,i+1}}{s+\tilde{a}_1} & \cdots & \frac{\tilde{b}_{1,n+1}}{s+\tilde{a}_1} \\ \frac{b_{2,1}}{s+a_2} & \frac{b_{2,2}}{s+a_2} & \cdots & \frac{b_{2,i+1}}{s+a_2} & \cdots & \frac{b_{2,n+1}}{s+a_2} \\ \vdots & \vdots & \ddots & \vdots & & \vdots \\ \frac{\tilde{b}_{2i-1,1}}{s+\tilde{a}_{2i-1}} & \frac{\tilde{b}_{2i-1,2}}{s+\tilde{a}_{2i-1}} & \cdots & \frac{\tilde{b}_{2i-1,i+1}}{s+\tilde{a}_{2i-1}} & \cdots & \frac{\tilde{b}_{2i-1,n+1}}{s+\tilde{a}_{2i-1}} \\ \frac{b_{2i,1}}{s+a_{2i}} & \frac{b_{2i,2}}{s+a_{2i}} & \cdots & \frac{b_{2i,i+1}}{s+a_{2i}} & \cdots & \frac{b_{2i,n+1}}{s+a_{2i}} \\ \vdots & \vdots & \ddots & \vdots & & \vdots \\ \frac{\tilde{b}_{2n-1,1}}{s+\tilde{a}_{2n-1}} & \frac{\tilde{b}_{2n-1,2}}{s+\tilde{a}_{2n-1}} & \cdots & \frac{\tilde{b}_{2n-1,i+1}}{s+\tilde{a}_{2n-1}} & \cdots & \frac{\tilde{b}_{2n-1,n+1}}{s+\tilde{a}_{2n-1}} \\ \frac{b_{2n,1}}{s+a_{2n}} & \frac{b_{2n,2}}{s+a_{2n}} & \cdots & \frac{b_{2n,i+1}}{s+a_{2n}} & \cdots & \frac{b_{2n,n+1}}{s+a_{2n}} \end{bmatrix} \times \begin{bmatrix} \delta\omega_c(s) \\ \delta\alpha_{v1}(s) \\ \vdots \\ \delta\alpha_{vi}(s) \\ \vdots \\ \delta\alpha_{vn}(s) \end{bmatrix} \tag{1}$$

where the compressor speed (ω_c) and the EEV openings (α_{v1}, α_{v2}, …, α_{vn}) are the inputs of total n rooms. The two-phase region temperatures (T_{e1}, T_{e2}, …, T_{en}), and the superheat temperatures (T_{sh1}, T_{sh2}, …, T_{shn}) are the outputs. δ is the slight disturbance around the equilibrium inputs and outputs. The coefficients of the first-order transfer functions are symbolled as $\tilde{a}$ and $\tilde{b}$ in the odd rows; a and b are in the even rows. However, the two-phase region temperatures of the evaporator are challenging to measure in experiments. In the odd columns of (1), T_{ei} is replaced by T_{ri}. In [2], the indoor thermal loads are ignored, and the heat exchange between the evaporator and room temperature is determined by the law of energy conservation:

$$C\frac{dT_r}{dt} = \dot{Q}_e. \tag{2}$$

$$C = \rho_{air} V_r K_{air} \tag{3}$$

$$\dot{Q}_e = \alpha_{e1}\pi D_e l_e (T_e - T_r) + \alpha_{e2}\pi D_e (L_e - l_e)(T_{es} - T_r) \tag{4}$$

where C is the indoor heat capacity, and $\dot{Q}_e$ is the heat transfer rate of the evaporator. ρ_{air}, V_r, K_{air}, α_{e1}, α_{e2}, D_e, l_e, L_e, and T_{es} are air density (kg/m^3), room size (m^3), the specific heat of air (J/kg·K), heat transfer coefficient in the two-phase region (W/K·Dm^2), heat transfer coefficient in the superheated zone (W/K·Dm^2), evaporator outer diameter (m), two-phase region length (m), total length of evaporator (m), and evaporator outlet temperature, respectively. The superheat temperature (T_{sh}) is defined as follows:

$$T_{sh} = T_{es} - T_e. \tag{5}$$

With the small variations $T_r \approx \delta T_r$, $T_e \approx \delta T_e$, and $T_{sh} \approx \delta T_{sh}$, and substituting (4) and (5) into (2), the small variation in room temperature δT_r is obtained:

$$\begin{aligned} \frac{d(\delta T_r)}{dt} = &-\frac{\pi D_e [\alpha_{e1} l_e + \alpha_{e2}(L_e - l_e)]}{C}\delta T_r \\ &+ \frac{\pi D_e [\alpha_{e2}(L_e - l_e)]}{C}\delta T_{sh} \\ &+ \frac{\pi D_e [\alpha_{e1} l_e + \alpha_{e2}(L_e - l_e)]}{C}\delta T_e \end{aligned} \tag{6}$$

Noting that the two-phase region occupies more than 90% of the total length of the evaporator, indicating L_e-$l_e \ll l_e$, the right-hand side of (6) can be neglected:

$$\frac{d(\delta T_r)}{dt} = -\frac{\alpha_{e1}\pi D_e l_e}{C}\delta T_r + \frac{\alpha_{e1}\pi D_e l_e}{C}\delta T_e. \tag{7}$$

The relationship between the temperature of the two-phase region and the room temperature is obtained by taking Laplace transform:

$$\delta T_r(s) = \frac{c_0}{s + c_0}\delta T_e(s). \tag{8}$$

where $c_0 = \alpha_{e1}\pi D_e l_e / C$

For the transfer function of odd rows in (1), δT_{ei} is substituted by δT_{ri} as follows:

$$\begin{aligned} \delta T_{ri}(s) = &\frac{\tilde{b}_{2i-1,1}}{s + \tilde{a}_{2i-1}}\frac{c_0}{s + c_0}\delta\omega_c(s) + \frac{\tilde{b}_{2i-1,2}}{s + \tilde{a}_{2i-1}}\frac{c_0}{s + c_0}\delta\alpha_{v1}(s) \\ &+ \ldots + \frac{\tilde{b}_{2n-1,2}}{s + \tilde{a}_{2n-1}}\frac{c_0}{s + c_0}\delta\alpha_{vn}(s). \end{aligned} \tag{9}$$

In [3], the pole value $\tilde{a}_{2i-1}$ is ten times greater than c_0; therefore, the pole c_0 can be considered the dominant pole to ignore the effect of $\tilde{a}_{2i-1}$. The dynamics of the inputs compressor speed and EEV openings to the outputs room and superheat temperatures are formulated as the equations of the

first-order system:

$$\begin{bmatrix} \delta T_{r1}(s) \\ \delta T_{sh1}(s) \\ \vdots \\ \delta T_{ri}(s) \\ \delta T_{shi}(s) \\ \vdots \\ \delta T_{rn}(s) \\ \delta T_{shn}(s) \end{bmatrix} = \begin{bmatrix} \frac{b_{1,1}}{s+a_1} & \frac{b_{1,2}}{s+a_1} & \cdots & \frac{b_{1,i+1}}{s+a_1} & \cdots & \frac{b_{1,n+1}}{s+a_1} \\ \frac{b_{2,1}}{s+a_2} & \frac{b_{2,2}}{s+a_2} & \cdots & \frac{b_{2,i+1}}{s+a_2} & \cdots & \frac{b_{2,n+1}}{s+a_2} \\ \vdots & \vdots & \ddots & \vdots & & \vdots \\ \frac{b_{2i-1,1}}{s+a_{2i-1}} & \frac{b_{2i-1,2}}{s+a_{2i-1}} & \cdots & \frac{b_{2i-1,i+1}}{s+a_{2i-1}} & \cdots & \frac{b_{2i-1,n+1}}{s+a_{2i-1}} \\ \frac{b_{2i,1}}{s+a_{2i}} & \frac{b_{2i,2}}{s+a_{2i}} & \cdots & \frac{b_{2i,i+1}}{s+a_{2i}} & \cdots & \frac{b_{2i,n+1}}{s+a_{2i}} \\ \vdots & \vdots & \ddots & \vdots & & \vdots \\ \frac{b_{2n-1,1}}{s+a_{2n-1}} & \frac{b_{2n-1,2}}{s+a_{2n-1}} & \cdots & \frac{b_{2n-1,i+1}}{s+a_{2n-1}} & \cdots & \frac{b_{2n-1,n+1}}{s+a_{2n-1}} \\ \frac{b_{2n,1}}{s+a_{2n}} & \frac{b_{2n,2}}{s+a_{2n}} & \cdots & \frac{b_{2n,i+1}}{s+a_{2n}} & \cdots & \frac{b_{2n,n+1}}{s+a_{2n}} \end{bmatrix} \times \begin{bmatrix} \delta\omega_c(s) \\ \delta\alpha_{v1}(s) \\ \vdots \\ \delta\alpha_{vi}(s) \\ \vdots \\ \delta\alpha_{vn}(s) \end{bmatrix}. \tag{10}$$

where

$$b_{2i-1,i+1} = \tilde{b}_{2i-1,i+1}c_i;$$
$$a_{2i-1} = c_i;$$
$$c_i = \left(\alpha_{e1}\pi D_e l_e / C\right)_i$$

The coefficient c_i is the heat transfer relation to the i^{th} evaporator in i^{th} room. The output modification of the transfer function makes the system measure only the room temperature and does not need to measure the temperature of the two-phase region of the evaporator. The system identification obtains the coefficients a_{2i-1}, a_{2i}, $b_{2i-1,i+1}$, and $b_{2i,i+1}$, where i= 1, 2, …, n, for total n numbers rooms. In [3], the linearized model in (10) is a system that is identified around the equilibrium output vector $\bar{\mathbf{x}} = \left[\bar{T}_{r1}\ \bar{T}_{sh1}\ \cdots\ \bar{T}_{rn}\ \bar{T}_{shn}\right]^T$ and the equilibrium input vector $\bar{\mathbf{u}} = \left[\bar{\omega}_c\ \bar{\alpha}_{v1}\ \cdots\ \bar{\alpha}_{vn}\right]^T$. The model employs a slight input disturbance to record a small output response when the system achieves stable values.

1) SYSTEM IDENTIFICATION

For the first-order system transfer function,

$$G_0(s) = \frac{b_0}{s + a_0} \tag{11}$$

where a_0 and b_0 are the parameters to be identified in the experiment, and a low-pass filter is utilized to reduce the noise in the experiment:

$$\lambda = \frac{1}{1 + \tau s} \tag{12}$$

where τ is the time constant.

Using (11) and (12), the transfer function is expressed as follows:

$$G_0(\lambda) = \frac{\beta_0\lambda}{1 + \alpha_0\lambda} \tag{13}$$

where $\alpha_0 = a_0\tau$-1, $\beta_0 = b_0\tau$. The time-domain responses are given by the following:

$$y_0(t) = -\alpha_0\left[\lambda y_0\right](t) + \beta_0\left[\lambda u_0\right](t) \tag{14}$$

where $[\lambda y_0]$ and $[\lambda u_0]$ are the filtered inputs and outputs.

The continuous time domain can be discredited from 0 to kT as the following matrix:

$$\mathbf{Y} = \boldsymbol{\varphi}\boldsymbol{\theta}, \tag{15}$$

where

$$\mathbf{Y}\left(\in \mathbb{R}^{(k+1)\times 1}\right) = \left[\, y_0(0)\ y_0(\mathrm{T})\ \cdots\ y_0(\mathrm{kT}) \,\right]^{\mathrm{T}}$$
$$\boldsymbol{\varphi}\left(\in \mathbb{R}^{(k+1)\times 2}\right) = \begin{bmatrix} -[\lambda y_0](0) & -[\lambda y_0](\mathrm{T}) & \cdots & -[\lambda y_0](\mathrm{kT}) \\ [\lambda u_0](0) & [\lambda u_0](\mathrm{T}) & \cdots & [\lambda u_0](\mathrm{kT}) \end{bmatrix}^{\mathrm{T}}$$
$$\boldsymbol{\theta}\left(\in \mathbb{R}^{2\times 1}\right) = \left[\, \alpha_0\ \beta_0 \,\right]^{\mathrm{T}}$$

The estimated parameter $\hat{\boldsymbol{\theta}}$ is obtained by the least squares method to identify a_0 and b_0 in the experiment as follows:

$$\hat{\boldsymbol{\theta}} = (\boldsymbol{\varphi}^{\mathbf{T}}\boldsymbol{\varphi})^{-1}\boldsymbol{\varphi}^{\mathbf{T}}\mathbf{Y}. \tag{16}$$

B. MODEL PREDICTIVE CONTROLLER DESIGN FOR THE VRF SYSTEM

MPC is featured in easy-to-incorporate constraints, such as maximum or minimum values for states, inputs, and rate limits. The physical constraints are directly used in controller design, ensuring that the superheat in the VRF system must always be greater than zero to prevent liquid refrigerant from entering the compressor and causing damage. (10) can be expressed as the state-space representation:

$$\delta\mathbf{x}(k+1) = \mathbf{A}\delta\mathbf{x}(k) + \mathbf{B}\delta\mathbf{u}(k) \tag{17}$$

where

$$\delta\mathbf{x}(k) = [\delta T_{r1}(k)\delta T_{sh1}(k)\cdots\delta T_{ri}(k)\delta T_{shi}(k)\cdots \delta T_{rn}(k)\delta T_{shn}(k)]^T;$$
$$\delta\mathbf{u}(k) = \left[\, \delta\omega_c(k)\ \delta\alpha_{v1}(k)\cdots\ \delta\alpha_{vi}(k)\cdots\ \delta\alpha_{vn}(k) \,\right]^T;$$
$$\mathbf{A}\left(\in \mathbb{R}^{2n\times 2n}\right) = \begin{bmatrix} -a_1 & \cdots & 0 \\ \vdots & \ddots & \vdots \\ 0 & \cdots & -a_{2n} \end{bmatrix};$$
$$\mathbf{B}\left(\in \mathbb{R}^{2n\times(n+1)}\right) = \begin{bmatrix} b_{1,1} & \cdots & b_{1,n+1} \\ \vdots & \ddots & \vdots \\ b_{2n,1} & \cdots & b_{2n,n+1} \end{bmatrix}.$$

For the present time, the MPC iterates the future responses in advance to optimize the input. Through accumulating the total output vector $\delta\mathbf{x}$ and input vector $\delta\mathbf{u}$ within the prediction horizon N_P from k to $k + N_p$, $\mathbf{A}$ and $\mathbf{B}$ form the

matrices within the control horizon N_C:

$$\begin{aligned}\delta\mathbf{X}(k+1) &\in \mathbb{R}^{(2n\cdot N_P)\times 1}\\ &= \begin{bmatrix}\delta\mathbf{x}(k+1)\\ \delta\mathbf{x}(k+2)\\ \vdots\\ \delta\mathbf{x}(k+N_P)\end{bmatrix} = \begin{bmatrix}\mathbf{A}\\ \mathbf{A}^2\\ \vdots\\ \mathbf{A}^{N_P}\end{bmatrix}\delta\mathbf{x}(k)\\ &+ \begin{bmatrix}\mathbf{B} & \mathbf{0} & \cdots & \mathbf{0}\\ \mathbf{AB} & \mathbf{B} & & \vdots\\ \vdots & \vdots & \ddots & \vdots\\ \mathbf{A}^{N_P-1}\mathbf{B} & \mathbf{A}^{N_P-2}\mathbf{B} & \cdots & \mathbf{AB}\end{bmatrix}\begin{bmatrix}\delta\mathbf{u}(k)\\ \delta\mathbf{u}(k+1)\\ \vdots\\ \delta\mathbf{u}(k+N_p-2)\end{bmatrix}.\end{aligned} \tag{18}$$

where $N_P = N_C+1$.

The output vector $\delta\mathbf{x}$ represents the response of the output state after the input from the previous state, while $\delta\mathbf{X}$ is a matrix formed by the accumulated output states over a period of time. The cost function of MPC is formed by the accumulated output matrix $\delta\mathbf{X}(k+1)$, tracking error, and constraints to obtain the optimized input at the $k+1$ moment. The first element $\delta\mathbf{u}(k)$ of the computed input vector at any sampling instant is the system input $\mathbf{u}_{\text{mpc}}$, and the remainder is discarded.

To make $\delta\mathbf{X}(k+1)$ approach the user-set temperatures $\hat{t}$, the target tracking function $\Delta\mathbf{T}(k+1)$ and two positive-definite matrices $\mathbf{Q_x}$, $\mathbf{R_u}$ are utilized to calculate the cost function J:

$$\begin{aligned}J = &[\delta\mathbf{X}(k+1) - \Delta\mathbf{T}(k+1)]^T\,\mathbf{Q}\,[\delta\mathbf{X}(k+1)\\ &-\Delta\mathbf{T}(k+1)] + \delta\mathbf{U}^T\mathbf{R}\delta\mathbf{U}\end{aligned} \tag{19}$$

where

$$\mathbf{Q}\left(\in \mathbb{R}^{(2n\cdot N_P)\times(2n\cdot N_P)}\right) = \begin{bmatrix}\mathbf{Q_x} & \mathbf{0} & \mathbf{0}\\ \mathbf{0} & \ddots & \mathbf{0}\\ \mathbf{0} & \mathbf{0} & \mathbf{Q_x}\end{bmatrix};$$

$$\mathbf{R}\left(\in \mathbb{R}^{[(n+1)\cdot(N_P-1)]\times[(n+1)\cdot(N_P-1)]}\right) = \begin{bmatrix}\mathbf{R_u} & \mathbf{0} & \mathbf{0}\\ \mathbf{0} & \ddots & \mathbf{0}\\ \mathbf{0} & \mathbf{0} & \mathbf{R_u}\end{bmatrix};$$

$$\begin{aligned}\Delta\mathbf{T}(k+1) &\in \mathbb{R}^{(2n\cdot N_P)\times 1}\\ &= \left[\,\Delta\mathbf{t}(k+1)\ \Delta\mathbf{t}(k+2)\ \cdots\ \Delta\mathbf{t}(k+N_P)\,\right]^T;\end{aligned}$$

$$\delta\mathbf{U}\left(\in \mathbb{R}^{[(n+1)\cdot(N_P-1)]\times 1}\right) = \begin{bmatrix}\delta\mathbf{u}(k)\\ \delta\mathbf{u}(k+1)\\ \vdots\\ \delta\mathbf{u}(k+N_p-2)\end{bmatrix};$$

$$\mathbf{Q_x}\left(\in \mathbb{R}^{2n\times 2n}\right) = \begin{bmatrix}W_{T_{r1}} & & \cdots & 0\\ & W_{T_{sh1}} & & \\ \vdots & & \ddots & \vdots\\ & & & W_{T_{rn}}\\ 0 & & \cdots & W_{T_{shn}}\end{bmatrix};$$

$$\mathbf{R_u}\left(\in \mathbb{R}^{(n+1)\times(n+1)}\right) = \begin{bmatrix}W_{\omega_c} & \cdots & 0\\ & W_{\alpha_{v1}} & \vdots\\ \vdots & & \ddots\\ 0 & \cdots & W_{\alpha_{vn}}\end{bmatrix}_{(n+1)\times(n+1)};$$

$$\Delta\mathbf{t} = \hat{\mathbf{t}} - \bar{\mathbf{x}} = \left[\,\Delta T_{r1}\ \Delta T_{sh1}\ \cdots\ \Delta T_{rn}\ \Delta T_{shn}\,\right];$$

$$\Delta T_r = \hat{T}_r - \bar{T}_r;\ \Delta T_{sh} = \hat{T}_{sh} - \bar{T}_{sh}.$$

The matrix $\Delta\mathbf{t}$ represents the difference between the user-set temperatures $\hat{t}$ and the equilibrium output vector $\bar{\mathbf{x}}$, which is the linearized point of the ($\mathbf{A}$, $\mathbf{B}$) model. The input and output weighting matrices $\mathbf{Q_x}$ and $\mathbf{R}_u$ are introduced in the cost function to balance the importance of adjusting inputs and outputs. The matrix form in (19) is formulated into cumulative form to facilitate calculation:

$$\begin{aligned}\mathbf{u}_{\text{mpc}} &= \arg\min_{\mathbf{u}(k)} J\\ &= \sum_{i=1}^{N_P-1}\left[\delta\mathbf{x}(k+i) - \Delta\mathbf{t}^t(k+i)\right]^T\mathbf{Q}_x\left[\delta\mathbf{x}(k+i) - \Delta\mathbf{t}^t(k+i)\right]\\ &\quad + \sum_{i=1}^{N_P-1}\delta\mathbf{u}(k+i-1)^T\mathbf{R}_u\delta\mathbf{u}(k+i-1)\\ &\quad \text{s.t. } \delta\mathbf{x}(k+i)\in\mathbb{X},\ \delta\mathbf{u}(k+i-1)\in\mathbb{U}\end{aligned} \tag{20}$$

The optimal input $\mathbf{u}_{\text{mpc}}$ is determined by minimizing J with the MPC's output and input constraints $\mathbb{X}$, $\mathbb{U}$ in the VRF system, promising positive superheat temperature to prevent liquid refrigerant from entering the compressor and causing equipment damage. This cost function J is modified to meet the iterative feasibility and asymptotic stability requirements in closed-loop MPC, ensuring that the terminal state $\mathbf{x}(k+N_P)$ remains within the terminal set. The entire process is repeated in the next time instant.

C. SUPERVISOR

Linearized models have been obtained for certain equilibrium output and input vectors $\bar{\mathbf{x}}, \bar{\mathbf{u}}$ in system identification. Supervisors switch between multiple reference models as optimization objectives for MPC. With a proper model, the MPC controls the VRF system to the linearized models' equilibrium output vectors by predicting and optimizing the future state. Because a linearized model is only used for describing linearized ranges around an equilibrium point, the supervisor dynamically selects an appropriate model for the MPC using algorithms to eliminate steady-state temperatures and compute mode-dependent dwell times in advance. This study proposes a method of using the supervisor for switching models within a limited number of linear models based on the current state.

1) STEADY-STATE TEMPERATURE ERROR ELIMINATION

For the linearized model established on the equilibrium point, the steady-state response can converge to the equilibrium

point under MPC control. According to the system identification in Section II-A, the linearized model ($\mathbf{A}_j$, $\mathbf{B}_j$) is a linear approximation within the range of $\bar{x} \pm \boldsymbol{\delta}\,\mathbf{x}$ and $\bar{u} \pm \boldsymbol{\delta}\,\mathbf{u}$. When the user-set temperature $\hat{\mathbf{t}}$ is not within the linear range, this model cannot calculate the correct input value, meaning it needs to switch others. However, when the user-set temperature is within the linear range of the model ($\mathbf{A}_j$, $\mathbf{B}_j$), but is not equal to $\bar{\mathbf{x}}$, the steady-state input must be calculated first as:

$$\begin{bmatrix} \mathbf{I}-\mathbf{A}_j & -\mathbf{B}_j \\ \mathbf{C} & \mathbf{0} \end{bmatrix} \begin{bmatrix} \hat{\mathbf{t}} \\ \mathbf{u}_{ss} \end{bmatrix} = \begin{bmatrix} \hat{\mathbf{0}} \\ \hat{\mathbf{t}} \end{bmatrix}$$
$$\text{where } \mathbf{C} = \mathbf{I} \in \mathbb{R}^{2n\times 2n};\ \mathbf{0} \in \mathbb{R}^{2n\times(n+1)};\ \hat{\mathbf{0}} \in \mathbb{R}^{(n+1)\times 1};$$
$$\hat{\mathbf{t}} = \begin{bmatrix} \hat{T}_{r1}\ \hat{T}_{sh1}\ \cdots\ \hat{T}_{rn}\ \hat{T}_{shn} \end{bmatrix}^T;$$
$$\mathbf{u}_{ss} = \begin{bmatrix} (\omega_c)_{ss}\ (\alpha_{v1})_{ss}\ (\alpha_{v2})_{ss}\ \cdots\ (\alpha_{vn})_{ss} \end{bmatrix}^T. \quad (21)$$

The least squares method is applied to solve $\hat{t}$ and $\mathbf{u}_{\text{ss}}$ in (21). If there is no solution, the MPC reference model must be switched. If the steady-state input $\mathbf{u}_{\text{ss}}$ exists, the user-set temperature is within the linear range of the reference model, and $\mathbf{u}_{\text{ss}}$ can be applied to eliminate the steady-state error. According to the user-set temperature $\hat{t}$, there may only a number of n_f ($n_f < m$) linearized models be solvable, with the solutions being $\mathbf{u}_{\text{ss}}$.

2) MODE-DEPENDENT DWELL TIME (MDT)

The mode-dependent dwell time (MDT) [29] is used for switching between appropriate linear models based on the states and the target. Before calculating the MDT, the feasible set X is introduced to determine the possible initial state $\mathbf{x}(k)$, which induces the terminal state $\mathbf{x}(k+N_p)$ to reach the stable equilibrium output vector $\bar{\mathbf{x}}$ of the model controlled by MPC, where the initial state $\mathbf{x}(k)$ is the summation of the input vector $\delta\mathbf{x}(k)$ and the equilibrium output vector $\bar{\mathbf{x}}$. By using (20) on the j^{th} model ($\mathbf{A}_j$, $\mathbf{B}_j$) (j= 1, 2, …, m), if the terminal state $\mathbf{x}_j(k+N_p)$, which is iterated from the initial state $\mathbf{x}_j(k)$, equals the stable equilibrium output vector $\bar{\mathbf{x}}_i$ ($i = 1, 2, \ldots, m$), the feasible initial state $\mathbf{x}_j(k)$ belong to the feasible set $\mathcal{X}_j(\bar{\mathbf{x}}_i)$.

The feasible set $\mathcal{X}_j(\bar{\mathbf{x}}_i)$ means the initial states $\mathbf{x}_j(k)$, iterated through the j^{th} model, will reach the equilibrium output vector $\bar{\mathbf{x}}_i$, identified by the i^{th} linearized model. Therefore, when the distance between the two equilibrium output vectors $\bar{\mathbf{x}}_1$ and $\bar{\mathbf{x}}_2$ is close, four feasible sets may exist: $\mathcal{X}_1(\bar{\mathbf{x}}_1)$, $\mathcal{X}_1(\bar{\mathbf{x}}_2)$, $\mathcal{X}_2(\bar{\mathbf{x}}_1)$, and $\mathcal{X}_2(\bar{\mathbf{x}}_2)$. The intersection of two models' feasible sets converged to $\bar{\mathbf{x}}_1$ is $\mathcal{X}_1(\bar{\mathbf{x}}_1) \cap \mathcal{X}_2(\bar{\mathbf{x}}_1)$ and converged to $\bar{\mathbf{x}}_2$ is $\mathcal{X}_1(\bar{\mathbf{x}}_2) \cap \mathcal{X}_2(\bar{\mathbf{x}}_2)$. The intersection of all models' feasible sets converged to $\bar{\mathbf{x}}_i$ can be determined as

$$\mathcal{X}_{\bar{\mathbf{x}}_i} = \bigcap_{j=1}^{m} \mathcal{X}_j(\bar{\mathbf{x}}_i). \quad (22)$$

Under the steady-state temperature error elimination and MPC optimization input calculation, the VRF system response controlled by the linearized model ($\mathbf{A}_j$, $\mathbf{B}_j$) at step H_j control is expressed as:

$$\mathbf{t}(k+H_j) = \mathbf{A}_j\mathbf{t}(k+H_j-1) + \mathbf{B}_j\mathbf{u}_{\text{act}}(k+H_j-1). \quad (23)$$

where

$$\mathbf{u}_{\text{act}} = \mathbf{u}_{\text{ss}} + \bar{\mathbf{u}}_j + \mathbf{u}_{\text{mpc}};$$
$$\mathbf{t} = \begin{bmatrix} T_{r1}\ T_{sh1}\ \cdots\ T_{ri}\ T_{shi}\ \cdots\ T_{rn}\ T_{shn} \end{bmatrix}^T$$

The difference between the state representations in (17) and (23) is that $\mathbf{t}(k+H_j)$ represents the system response captured from the temperature sensors in the VRF system at the H^{th} moment. For the $\delta\mathbf{x}(k+1)$ in (17), it only represents the state output obtained from the state at k moment via the input $\delta\mathbf{u}(k)$. The response $\mathbf{t}(k+H_j)$ is controlled by the sum of optimized input $\mathbf{u}_{\text{mpc}}$ with the j^{th} model, the equilibrium input vector $\bar{u}_j$ of the model ($\mathbf{A}_j$, $\mathbf{B}_j$), and the steady-state input $\mathbf{u}_{\text{ss}}$.

Using (22) and (23), the MDT $H_{j,i}$ can be defined as the number of step counts for a VRF system controlled by the j^{th} model when the $\mathbf{t}(k+H_{j,i})$ is a superset of $\mathcal{X}_{\bar{\mathbf{x}}_i}$, as the following condition:

$$\mathbf{t}(k+H_{j,i}) \subseteq \mathcal{X}_{\bar{\mathbf{x}}_i}. \quad (24)$$

The MDT can calculate the time required to switch between models. Switching is only permitted when the time exceeds the MDT, and a more suitable model describes the VRF system. The theoretical approach requires calculating the MDT for each model switch, which consumes excessive computational resources in real-time control. Precomputing and storing the results of MDTs saves computational time and ensures the feasibility of system switching. Therefore, the number of preprocessed MDTs can be obtained for each model at all user-set temperatures. MDT is essential to prevent the switching frequency from becoming excessively fast and ensure switching stability. If two models are established with equilibrium room temperatures of 27°**C** and 25°**C**, respectively, the number of MDT step counts required to reach 26°**C** can be calculated by (24). When the user sets the temperature to 26°C, existing MDTs $H_{27°\mathbf{C},26°\mathbf{C}}$ and $H_{25°\mathbf{C},26°\mathbf{C}}$, the two models might switch frequently because the temperature of both models differs by one degree relative to 26°C; therefore, the supervisor model-switch strategy is proposed to switch a reference model for MPC dynamically.

3) SUPERVISOR MODEL-SWITCH STRATEGY

Fig. 3 shows the supervisor model-switch strategy flow chart for the VRF system. First, the pre-established data are initialized, as shown in Fig. 3(a). When identifying the system for a quantity of m room temperatures, linearized models ($\mathbf{A}_j$, $\mathbf{B}_j$) (j= 1, 2, …, m) are obtained in the form of (10) for each of the equilibrium output vectors $\bar{\mathbf{x}}_j$ and input vectors $\bar{\mathbf{u}}_j$. Feasible sets and intersections are established through (20) and (22) to check whether the equilibrium output vector of the i^{th} model $\bar{\mathbf{x}}_i$ will reach as MPC's reference model is j^{th} model. The next step calculates MDTs $H_{j,i}$, the number

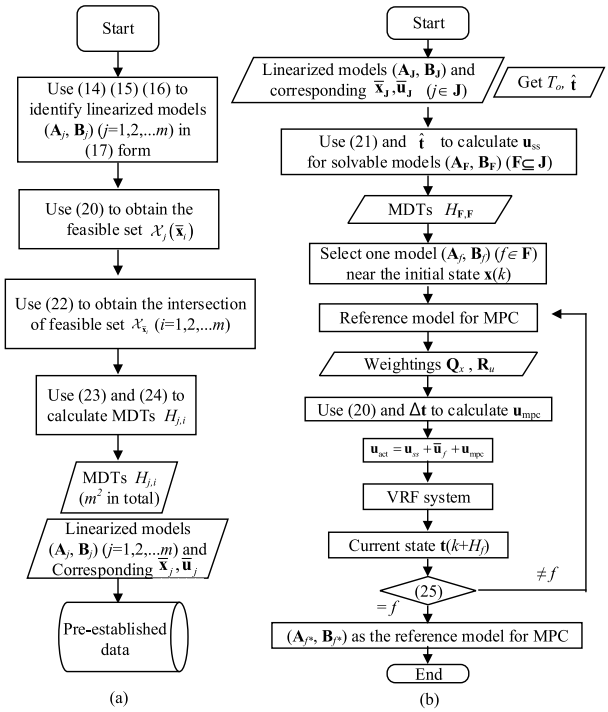

FIGURE 3. The flowchart of the supervisor model-switch strategy. (a) Pre-established data. (b) Supervisor model-switch strategy.

of steps required to switch between models, indicating the availability of the switch model when the steps exceed MDTs. Therefore, the MDTs and linearized models are saved to load for the real-time VRF system, as shown in Fig. 3(b).

After the user activates the VRF system, the supervisor obtains the user-set temperatures $\hat{t}$ and outdoor temperature T_o, and the set of linearized models ($\mathbf{A_J}$, $\mathbf{B_J}$) ($\mathbf{J}$= {1,2,...}, $|\mathbf{J}| = m$) with different equilibrium output vector $\bar{\mathbf{x}}_\mathbf{J}$ and input $\bar{\mathbf{u}}_\mathbf{J}$. The first step in the experimental process is to eliminate the steady-state temperature error and to obtain steady-state inputs $\mathbf{u}_{ss}$ by calculating (21) if solvable.

The next step is to load MDT and choose one model ($\mathbf{A}_f$, $\mathbf{B}_f$) from the solvable models, denoted as ($\mathbf{A_F}$, $\mathbf{B_F}$) ($\mathbf{F} \subseteq \mathbf{J}, |\mathbf{F}| = n_f < m$), in which the distance between the initial temperature $\mathbf{t}(k)$ and the equilibrium output vector $\bar{\mathbf{x}}_f$ is shortest. The next step is to choose one model ($\mathbf{A}_f$, $\mathbf{B}_f$) as the reference model for MPC. The user-set weighting matrices $\mathbf{Q}_\mathrm{x}$ and $\mathbf{R}_\mathrm{u}$ are transmitted to the cost function (20) for solving optimized $\mathbf{u}_{\mathrm{mpc}}$. The actual inputs $\mathbf{u}_{\mathrm{act}}$, summing of $\mathbf{u}_{\mathrm{ss}}$, $\mathbf{u}_{\mathrm{mpc}}$, and $\bar{\mathbf{u}}_f$, input to the VRF system.

Once the current temperature $\mathbf{t}(k + H_f)$ is close to another equilibrium output vector $\bar{\mathbf{x}}_{f*}$ ($f* \neq f$) and the iteration H_f is larger than MDT, the reference model f will switch until the correct model $f*$. The following equation guarantees that switching is available when the number of steps H_f in the current state is greater than MDT:

$$f* = \arg\min_{f*(\in\mathbf{F})} \left(\left\| \mathbf{t}\left(k + H_f\right) - \bar{\mathbf{x}}_\mathbf{F} \right\| \right)$$
$$\text{s.t. } H_f > H_{f,f*} \tag{25}$$

This approach allows for controlling the same target temperature by switching between multiple mathematical models, prevents the switching frequency from becoming excessively fast, and ensures switching stability. The switching occurs when the accumulated residence time of a particular model exceeds the set residence time, guaranteeing the switching frequency and the continuous feasibility of MPC. Due to the susceptibility of room and superheat temperatures to various factors, the decision to switch models depends on the residence time being greater than the set value. The state must enter the feasible set corresponding to the model to ensure stable switching.

III. NUMERICAL VERIFICATIONS AND ILLUSTRATIVE APPLICATIONS

The use of MPC with the supervisor modelswitch strategy for controlling the VRF system is numerically verified through the following three focuses:

1) Numerical verification of system identification for the commercial one-to-three VRF system. Three different equilibrium room temperatures at 26.5°C, 25°C, and 23.5°C are operated to obtain the transfer function matrices, verifying the match of output responses when the same situation and inputs are in the experiment.

2) Numerical investigation exploring the effect of MPC weighting parameters $\mathbf{Q}_\mathrm{x}$ and $\mathbf{R}_\mathrm{u}$.

3) Numerical validation of the supervisor model-switch strategy on the VRF system through setting room temperatures from 26.5°C through 25°C to 23.5°C in sequence.

A. NUMERICAL VERIFICATION OF SYSTEM IDENTIFICATION ON THE VRF SYSTEM

The system identification process involves giving steady inputs, waiting for the system to reach equilibrium, and applying input disturbances of square waveforms. According to the filtered input and output responses by (14) in the time domain, the transfer function matrices are obtained in the form of (10) using the system identification technique. The different equilibrium output and input vectors lead to multiple linearized models. In the experiments with the one-to-three VRF system, the linearized models are identified based on the room temperature (T_r) and superheat temperature (T_{sh}) in equilibrium output vector $\bar{\mathbf{x}}$, and the EEV opening (α_v) and compressor speed (ω_c) as equilibrium input vector $\bar{\mathbf{u}}$ are listed in Table 2. The configuration of the rooms is shown in Fig. 1(a). The linearized models are formulated by tuning the inputs of α_v and ω_c to operate the three rooms at steady-state temperatures of 26.5°C, 25°C, and 23.5°C. Since the objective of this experiment is to control the room temperature while ensuring that the superheat remains above 0°C, the focus of the output operating point lies primarily on the room temperature.

The experimental parameters of the environment and thermal loads for the VRF system are listed in Table 3. An evaporator corresponding to the cooling capacity of the room size was installed in each room. Room 5 was installed

TABLE 2. Operating points for system identification.

Num	State $\bar{\mathbf{x}}$		Input $\bar{\mathbf{u}}$	
	T_r (℃)	T_{sh} (℃)	α_v (*pulse*)	ω_c (*rps*)
Experiment 1: 26.5°C				
①	26.5	14	143	27
②		13	199	
③		13	330	
Experiment 2: 25°C				
Num	T_r (℃)	T_{sh} (℃)	α_v (*pulse*)	ω_c (*rps*)
①	25	17	165	43
②		17	200	
③		17	385	
Experiment 3: 23.5°C				
Num	T_r (℃)	T_{sh} (℃)	α_v (*pulse*)	ω_c (*rps*)
①	23.5	16.2	300	60
②		17.3	250	
③		18	350	

TABLE 3. Experimental parameters for the VRF system.

Environment Variable			Thermal loads (*kW*)		
Num	Size	Capability	Exp. 1	Exp. 2	Exp. 3
①	5.14 (*py*)	3.6 (*kW*)	2.75	2	2.75
②	5.56 (*py*)	4.5 (*kW*)	1.5	1.5	1.5
③	8.19 (*py*)	5 (*kW*)	2.75	1.75	1.75
⑤	Outspace	14(*kW*)	Fixed 35°C		

with a condenser with a 14 kW cooling capacity and an environmental control system that served as the test facility to maintain a temperature of 35°C, simulating the outdoor space. In addition, heat loads of 1.5 to 2.75 kW were added to the experiments to simulate the actual situation of people as a heat source and compensate for environmental temperature variations while maintaining steady-state room temperatures.

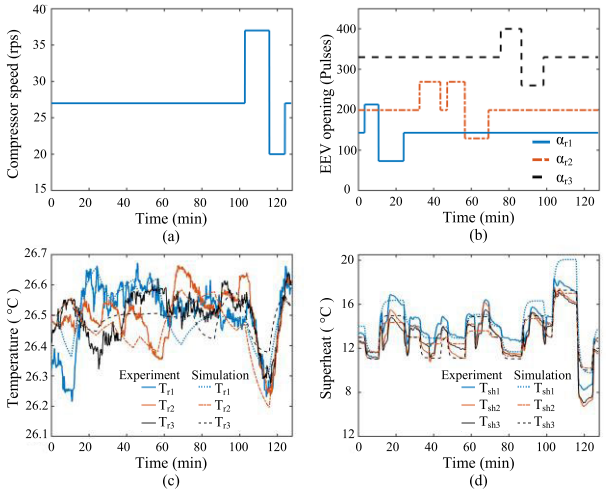

FIGURE 4. System identification results at the 26.5°C room temperature operating point. (a) System input response of compressor speed. (b) System input response of the EEV opening. (c) Room temperature response. (d) Superheat response.

Figs. 4 to 6 illustrate the input and corresponding output responses for the three experiments at 26.5°C, 25°C, and 23.5°C room temperature operating points using the system identification results to verify the match of transfer functions.

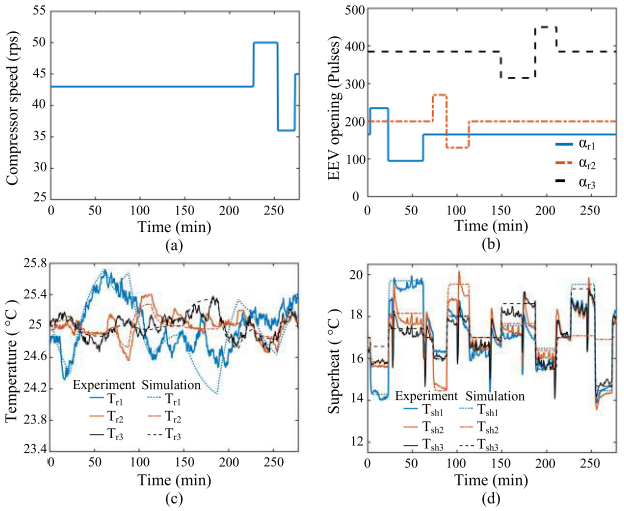

FIGURE 5. System identification results at the 25°C room temperature operating point. (a) System input response of compressor speed. (b) System input response of the EEV opening. (c) Room temperature response. (d) Superheat response.

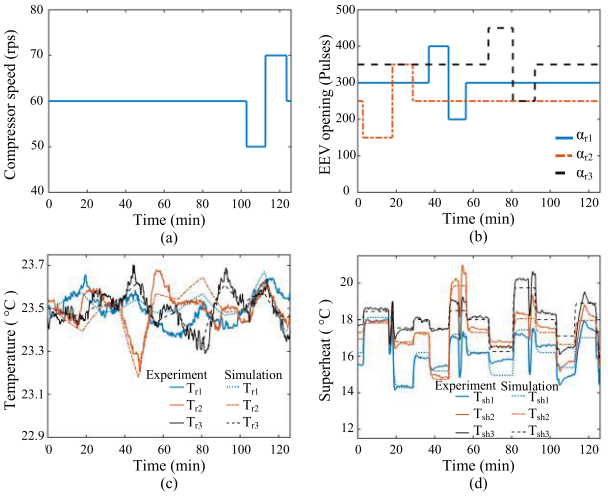

FIGURE 6. System identification results at the 23.5°C room temperature operating point. (a) System input response of compressor speed. (b) System input response of the EEV opening. (c) Room temperature response. (d) Superheat response.

The simulated parameters are listed in Tables 2 and 3. The experimental times of Fig. 4 to 6 are 127 minutes, 277 minutes, and 125 minutes, respectively. For Fig. 4(a), (b) to Fig. 6(a), (b), the inputs of compressor speed and EEV openings are given complete square waves in sequence to separate and identify each input effect. Before starting the following input, the previous input and state will wait for the return to equilibrium to prevent affecting the next state. The output responses of room and superheat temperatures are shown in Fig. 4(c), (d), Fig. 5(c), (d), Fig. 6(c), (d), which include experimental and simulated data. The first-order transfer function listed in Table 4 was obtained using the system identification technique on the inputoutput curves of the experimental data. Fig. 4(c), (d) show the simulated

and experimental room and superheat temperature responses. When only one EEV opening becomes larger with the others unchanged, the other room temperatures increase, and the superheat decreases. The situation is caused by more refrigerant flowing in that evaporator, and the others decreased. Experiments 2 and 3 were also conducted to identify the room temperatures at 25°C and 23.5°C. The results are shown in Figs. 5 and 6, with the identified parameters listed in Table 4.

TABLE 4. Model parameters for the VRF system.

26.5°C room temperature model					
a_1	a_2	a_3	a_4	a_5	a_6
-0.00241	-0.0153	-0.00198	-0.0200	-0.00458	-0.02126
$b_{1,1}$	$b_{2,1}$	$b_{3,1}$	$b_{4,1}$	$b_{5,1}$	$b_{6,1}$
-5.2e-5	0.0092	-7.5e-5	0.00802	-5.8e-5	0.0090
$b_{1,2}$	$b_{2,2}$	$b_{3,2}$	$b_{4,2}$	$b_{5,2}$	$b_{6,2}$
-7.19e-6	-0.00051	2.76e-6	-0.00039	3.61e-6	-0.00059
$b_{1,3}$	$b_{2,3}$	$b_{3,3}$	$b_{4,3}$	$b_{5,3}$	$b_{6,3}$
4.812e-6	-0.00023	-4.08e-6	-0.00017	4.303e-7	-0.00057
$b_{1,4}$	$b_{2,4}$	$b_{3,4}$	$b_{4,4}$	$b_{5,4}$	$b_{6,4}$
4.06e-7	-0.00051	2.613e-6	-0.00049	-5.37e-6	-0.00059
25°C room temperature model					
a_1	a_2	a_3	a_4	a_5	a_6
-0.00075	-0.04055	-0.00288	-0.02498	-0.00206	-0.04291
$b_{1,1}$	$b_{2,1}$	$b_{3,1}$	$b_{4,1}$	$b_{5,1}$	$b_{6,1}$
-6.25e-5	0.01472	-5.85e-5	0.000306	-5.05e-5	0.01427
$b_{1,2}$	$b_{2,2}$	$b_{3,2}$	$b_{4,2}$	$b_{5,2}$	$b_{6,2}$
-1.07e-5	-0.00157	3.46e-6	-0.00041	3.946e-6	-0.00026
$b_{1,3}$	$b_{2,3}$	$b_{3,3}$	$b_{4,3}$	$b_{5,3}$	$b_{6,3}$
9.571e-6	-0.00060	-1.19e-5	-0.00091	1.511e-6	-0.00061
$b_{1,4}$	$b_{2,4}$	$b_{3,4}$	$b_{4,4}$	$b_{5,4}$	$b_{6,4}$
1.108e-5	-0.00032	1.52e-6	-0.00024	-1.03e-5	-0.00099
23.5°C room temperature model					
a_1	a_2	a_3	a_4	a_5	a_6
-0.00097	-0.02995	-0.00066	-0.02857	-0.00194	-0.0622
$b_{1,1}$	$b_{2,1}$	$b_{3,1}$	$b_{4,1}$	$b_{5,1}$	$b_{6,1}$
-4.06e-5	0.002438	-2.85e-5	0.00189	-1.77e-5	0.00558
$b_{1,2}$	$b_{2,2}$	$b_{3,2}$	$b_{4,2}$	$b_{5,2}$	$b_{6,2}$
-1.17e-6	-0.00057	1.537e-6	-0.00015	8.245e-6	-0.00028
$b_{1,3}$	$b_{2,3}$	$b_{3,3}$	$b_{4,3}$	$b_{5,3}$	$b_{6,3}$
1.107e-6	-0.00030	-6.44e-6	-0.00073	3.307e-6	-0.00031
$b_{1,4}$	$b_{2,4}$	$b_{3,4}$	$b_{4,4}$	$b_{5,4}$	$b_{6,4}$
1.335e-6	-0.00037	1.978e-6	-0.00022	-4.07e-6	-0.00109

The large room temperature oscillation responses in Fig. 4(c), Fig. 5(c), and Fig. 6(c) are caused by people entering the room. In addition, according to the same row in (10), a single output is contributed by summing the transfer functions with the same pole for all inputs. During the system identification, the pole with a smaller fitting error will be selected to present the effect of the whole input to the output. Under this balance consideration, there will be a gap between the simulation and experimental responses. The transfer function matrices obtained from the system identification were utilized for the following controller design to verify the MPC feasibility further.

B. NUMERICAL VERIFICATION OF MODEL PREDICTIVE CONTROL FOR VRF SYSTEM

Simulations were conducted to investigate the response of the room and superheat temperatures in the VRF system. The objective is to achieve the user-set room temperatures of 25°C in three rooms controlled by the 25°C room temperature model. Considering that reducing superheat can enhance energy efficiency, two sets of controllers with different superheat weighting matrices, $\mathbf{Q}_x$ and $\mathbf{R}_u$ referred to (20), were designed and are listed in Table 5. The selection of the weighting matrices in the cost function is primarily based on multiple simulations to adjust the parameters that best align with the set objectives, including convergence time and steady-state error. Two different weighting matrices for the superheat, aiming to analyze the differences in the corresponding room temperature and superheat response, are compared.

TABLE 5. The parameters of the weighting matrices for the model predictive controller.

MPC1	
$\mathbf{Q}_x$	$\mathbf{R}_u$
diag([300,0.01,300,0.01,300,0.01])	diag([0.5,0.5,0.5,1])
MPC2	
$\mathbf{Q}_x$	$\mathbf{R}_u$
diag([300,50,300,50,300,50])	diag([0.5,0.5,0.5,1])

Since the VRF system is a slower response system, setting a faster sampling time would lead to system input oscillations and poor state response performance. In system identification, the transient response of the VRF system determines the appropriate sampling time duration. For the identified process of the room temperature of 26.5°C, in Fig. 4(b), a complete input square wave α_{v1} ranging from 5 minutes to 25 minutes in duration is provided, and the corresponding experimental outputs T_{sh} are shown in Fig. 4(d). The input-output signal allows the calculation of a delay time of approximately 40 seconds for the square wave. Therefore, the sampling time for the controller is set to 40 seconds, with a prediction horizon N_P of 20 sampling times and a control horizon N_c of 19 sampling times. By predicting the system's state output over a more extended period, the system inputs can be adjusted based on the results to achieve smoother system state outputs.

Fig. 7 and Fig. 8 show simulation results of the controller weighting parameters on MPC within 50 minutes. The compressor speed and EEV opening input are shown in Fig. 7(a), (b) and Fig. 8(a), (b). The initial conditions for all room temperatures were 30°C; user-set room and superheat temperatures were set to 25°C and 17°C. Constraints were incorporated into the MPC, including input constraints $\mathbb{U}$, such as the EEV opening limited between 130 and 400 pulses and the compressor speed limited between 20 and 64 rps. The room temperature and superheat output are shown in Fig. 7(c), (d), and Fig. 8(c), (d). Regarding the state response constraint $\mathbb{X}$, the superheat is required to remain above 0°C to ensure the safety of the compressor equipment.

As shown in Fig. 7, the MPC2 places a higher weight on the superheat, causing the demand to simultaneously

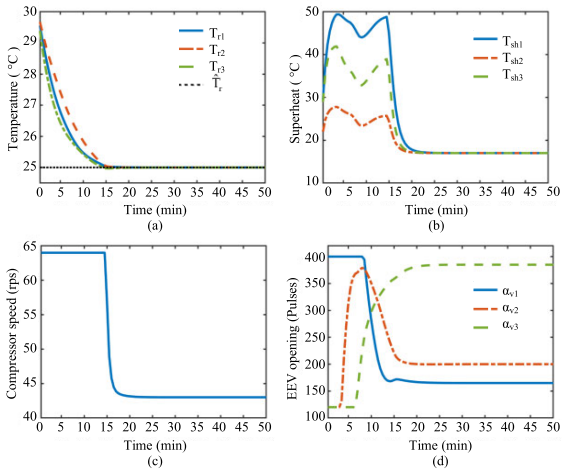

FIGURE 7. Model predictive controller simulation with low superheat weight. (a) Room temperature response. (b) Superheat response. (c) System input response of compressor speed. (d) System input response of the EEV opening.

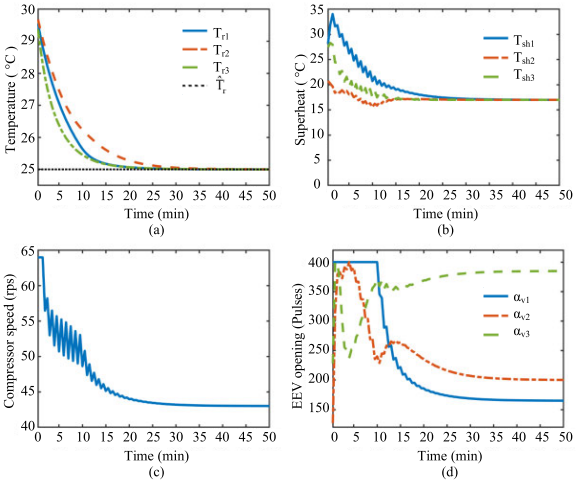

FIGURE 8. Model predictive controller simulation with a high superheat weight. (a) Room temperature response. (b) Superheat response; (c) System input response of compressor speed. (d) System input response of the EEV opening.

track the room temperature and converge the superheat to the user-set temperature. This design leads to oscillations in the compressor input, resulting in a higher load on the compressor than on the MPC1. Additionally, the early decrease in compressor speed causes a slower convergence of the room temperature. Fig. 7(a) and Fig. 8(a) demonstrate that MPC1 aligns better with the research objective, allowing full-speed cooling until the room temperature reaches the target value and reducing the superheat to minimize energy consumption. Comparing Fig. 7(c), (d) and Fig. 8(c), (d), since MPC1 does not need to track the superheat and room temperature at the same time, the input changes of the latter are smoother and can avoid system input oscillation. Therefore, the weight parameters of MPC1 were used in this study.

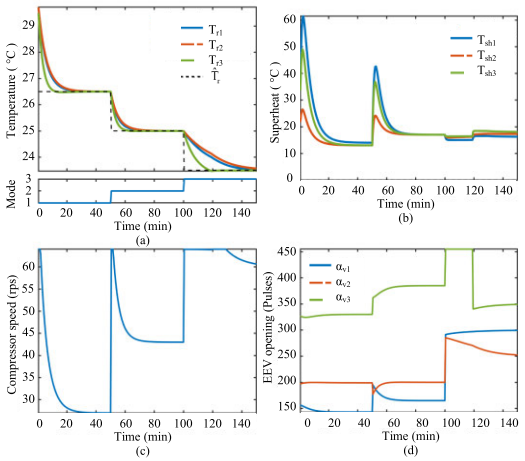

FIGURE 9. Model predictive controller simulation with model-switching strategy. (a) Room temperature and switching mode. (b) Superheat response. (c) Compressor speed. (d) EEV opening.

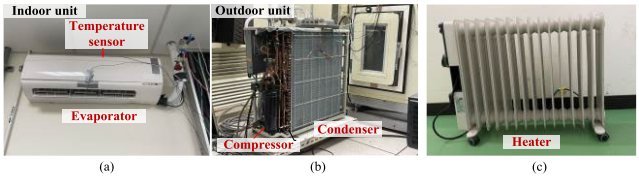

FIGURE 10. Experimental setup. (a) Indoor unit. (b) Outdoor unit; (c) Heater.

C. NUMERICAL VALIDATION OF THE SUPERVISOR MODEL-SWITCH STRATEGY ON THE VRF SYSTEM

The linearized models and proper MPC's parameters $\mathbf{Q}_x$ and $\mathbf{R}_u$, referred to Table 4 and 5, have been proposed in Sections III-A and III-B. The supervisor model-switch strategy is essential to validate room temperature and superheat control according to the distance between the current states and equilibrium output vectors.

Fig. 9 shows the simulation results of the MPC controller using the model-switch strategy. Based on the limitations of the VRF system, the upper and lower constraints of EEV opening are setting 450 pulses and 130 pulses, and the compressor speeds are setting 64 rps and 20 rps. Three rooms' temperatures are controlled at 26.5°C, 25°C, and 23.5°C in sequence; furthermore, by changes in temperature settings, the supervisor model-switch strategy automatically changes reference models, as shown in Fig. 9(a). Fig. 9(b) displays the simulation results for the superheat temperature, with all superheat values above 0°C and meeting the specified requirements. It can be observed that the increase in compressor speed during model switching leads to an increase in superheating. Fig. 9(c) illustrates the increase in compressor speed when switching models and the gradual decrease when the target temperature is close. However, during the transition from 25°C to 23.5°C, the temperature reduction is slow because the compressor speed limit is 64 rps. Fig. 9(d) presents the simulation results for the EEV opening

input. Under variations in input constraints and temperature settings, it is demonstrated that the supervisor model-switch strategy can be applied to a one-to-three VRF system, smoothly transitioning between different linear models in the MPC controller, maintaining the target temperatures at 26.5°C, 25°C, and 23.5°C while keeping superheat above 0°C.

IV. EXPERIMENT

The proposed control method for a one-to-three system in Fig. 2(c) has been experimentally investigated. Two experiments were conducted to validate the proposed supervisor model-switch strategy. The first one validates the feasibility of the MPC method on a one-to-three VRF system to track the desired single-point target temperature on different temperature models. The second experiment investigates to validate whether the supervisor model-switch strategy can smoothly transition models and control the room temperature at the user-set temperatures.

TABLE 6. Thermal loads for the experiment.

Num.	Exp. 1	Exp. 2
①	2 kW	2.75 kW
②	1.5 kW	1.5 kW
③	1.75 kW	1.75 kW
⑤	Fixed 35°C	

A. MODEL PREDICTIVE CONTROLLER ON ONE-TO-THREE VRF SYSTEM

Fig. 1(a) shows the relative room location in the experiment. The space sizes, evaporator capacities, and condenser capacity of each room are listed in Table 3. The walls of each room were made of steel and cement, and the color of the walls was white. The experimental equipment is shown in Fig. 10. The evaporator and EEV were installed in the indoor unit, above which the temperature sensor was located at the inlet, as shown in Fig. 10(a). The thermal loads of the four indoor units for the two experiments are shown in Table 6. To simulate the outdoor environment, an environmental control system was used to fix the room temperature at 35 °C. In particular, the walls of room 5 are covered with thermal insulation paper to prevent them from affecting other rooms with indoor units. The outdoor unit comprised a compressor and a condenser, as shown in Fig. 10(b). As shown in Fig. 10(c), the heater provided heat sources from 1 kW to 3 kW, and the experimental refrigerant was R-410A. The thermal loads were located at the center of each room, primarily aimed to compensate for room temperatures and achieve consistent environmental conditions across different rooms. The execution time with a PC (Intel Core i7-1280P, 32-GB SRAM, 64-bit OS) is 1.6 seconds. In addition, several uncertain heat sources exist in the experimental environment, further complicating the controller design. Another important mechanism of the VRF system is lubrication oil return, in which oil accumulates in the pipelines of the closed indoor units under a partial load to lubricate the compressor. To stabilize the system operation, the closed EEV had to open and increase the compressor speed to lubricate the oil returning to the compressor. However, this mechanism leads to a sudden decrease in superheat and a reduction in cooling capacity. These circumstances present challenges in the controller's design, highlighting the controller's significance in effectively addressing such situations.

For the experimental validation of the MPC, the experiment controlled the room temperatures from 28.3°C to 26°C within a deviation of less than 0.5°C and maintained the superheat above 0°C. Following the flowchart of the supervisor model-switch strategy in Fig. 3(b), the 26.5°C models were selected to describe the reference model, and user-set temperatures $\hat{\mathbf{t}}$ of the three rooms were set to [26°C, 0°C, 26°C, 0°C, 26°C, 0°C]. The temperature difference $\Delta\mathbf{t}$ can be obtained according to the 26.5°C model as [0.5°C, 0°C, 0.5°C, 0°C, 0.5°C, 0°C]. The steady-state temperature $\mathbf{u}_{ss}$ is calculated by (21). Since this experiment didn't require switching to another model, the model f selected at the beginning was $f*$. With the parameters $\mathbf{Q}_x$ and $\mathbf{R}_u$, the next step was to solve $\mathbf{u}_{mpc}$ using (20). The lower limit of the EEV opening was set as 130 pulses to ensure enough refrigerant flowing into the evaporator. The upper limit of the EEV opening was set as 400 pulses to reduce the superheat temperature and reduce energy consumption in the control process. Fig. 11 represents the experimental results of the model predictive controller, with an experimental duration of 85 minutes. Fig. 11 (a) is the room temperature output, Fig. 11 (b) is the superheat output, and the dashed line represents the lower limit of the superheat. The values of the compressor speed and EEV opening obtained by the MPC are demonstrated in Fig. 11(c), (d). The experimental results showed that the system achieved the target temperature within 40 minutes when the compressor operated at full speed. Due to an upper limit on the compressor speed, the hardware of the VRF system was protected. Due to superheat limits being included in the MPC, the system adjusted the compressor and EEV to control the superheat above the lower limit, as shown in Fig. 11(b). The oil return mechanism was initiated at 20 and 58 minutes, as shown in Fig. 11(d).

Nevertheless, after the oil returned, the MPC adjusted the system input to maintain a steady room temperature. The steady-state room temperature errors were 0.09°C, 0.09°C, and 0.17°C for three rooms, respectively. The room temperature errors for each room were below 0.2°C, which aligns with expectations and signifies that the MPC effectively maintains a room temperature close to the target temperature.

B. MODEL PREDICTIVE CONTROLLER WITH SUPERVISOR MODEL-SWITCH STRATEGY ON ONE-TO-THREE VRF SYSTEM

The proposed supervisor model-switch strategy can expand a single-point temperature control to achieve different user-set temperatures in each room. In the experiments, the initial

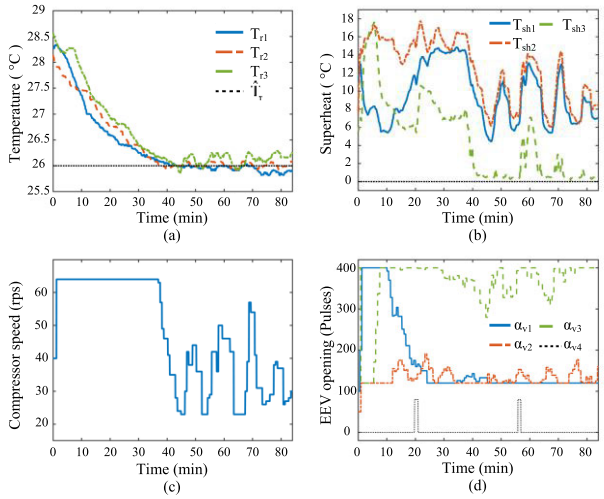

FIGURE 11. Model predictive controller experiment for the 26°C target temperature. (a) Temperature. (b) Superheat. (c) Compressor speed. (d) EEV opening.

room temperatures for Room 1, Room 2, and Room 3 are 31°C, 29°C, and 28°C, respectively. The temperatures controlled by the three rooms are divided into two parts. In the first part, the temperatures controlled by the three rooms were the same, which were 26°C, 25°C, and 24°C, respectively. In the second part, the temperature of the second room was set as 23°C, while the other rooms were 24°C. Various models correspond to different model predictive controllers. Model 1 used a 26.5°C room temperature model, Model 2 used a 25°C indoor temperature model, and Model 3 used a 23.5°C indoor temperature model. The MDT was set at five sampling times.

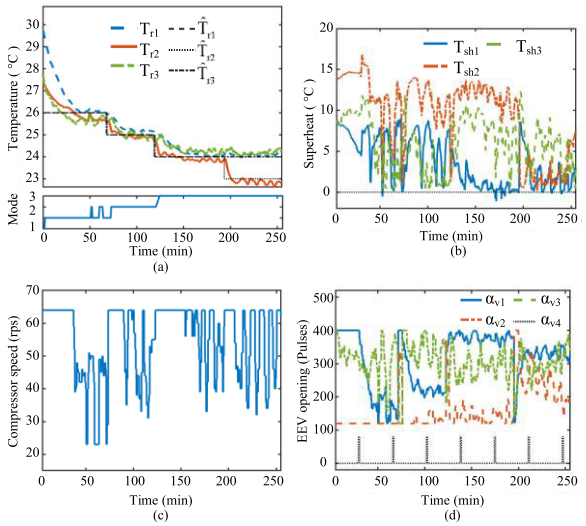

FIGURE 12. Experimental results of the model predictive controller with the supervisor model-switch strategy. (a) Room temperature response with mode selection; (b) Superheat response; (c) Compressor speed; (d) EEV opening.

The experimental results, as shown in Fig. 12, revealed six model switchings during the process, and the total duration of the experiment was 250 minutes. In this experiment, it was observed that for the same user-set temperature of 26°C, Model 1 could not control the steady-state error to be within 0.5°C, leading to a switching event. Due to the considerable disparity between the thermal load configuration used in the experiment and the thermal load configuration estimated by Model 1, a model mismatch scenario emerged. Fig. 12(a) shows the room temperature response and model switching. Fig. 12(b) shows the superheat response above the lower limit (dashed line) with MPC. However, when the occasional instances fell below the lower limit, the controller promptly increased the superheat by adjusting the compressor and EEV input to prevent the liquid refrigerant from entering the compressor. Fig. 12(c) and Fig. 12(d) show each room's inputs for the compressor and the EEV opening, respectively. The steady-state errors from the experiments are listed in Table 7. The experimental results indicate that using the supervisor model-switch strategy makes controlling the same user-set temperature possible using different models, thereby mitigating the risk of model mismatch. The system operated stably and precisely controlled the room temperature at the target value, with a steady-state error within 0.5°C. The experimental results align with expectations, demonstrating the system's ability to maintain stable temperature control and decrease uncertainties in heat sources.

TABLE 7. Steady-state error of room temperature for Experiment 2.

User-set temperature	T_{r1} (°C)	T_{r2} (°C)	T_{r3} (°C)
26°C	0.16	0.27	0.33
25°C	0.22	0.12	0.42
24°C	0.12	0.15	0.27
24°C and 23°C	0.15	0.17	0.27

TABLE 8. System specifications.

	[14]	[21]	This work
Plant	Variable air volume	one-to-three VRF	one-to-three VRF
Modeling method	Support vector regression	Finite control volume approach	Least squares
MPC method	Centralized	Supervisory Decentralized	Supervisory Centralized
Settling time (sec)	About 1500	About 2500	About 2100
Temperature steady-state error (°C)	0.18	About 0.5	Less than 0.5

Table 8 summarizes the performance parameters of the proposed supervisor model-switch strategy in MPC of the variable flow system fields. In [14], centralized MPC was implemented in the variable air volume system with 1500 seconds settling time and 0.18°C temperature error in the steady state. For the slower-response one-to-three VRF plant compared to air volume control in [21], the supervisor decentralized MPC was applied to calculate evaporator cooling and pressure setpoints for each zone with the settling

time larger about 2500 seconds and the temperature error of 0.5°C. The proposed supervisor model-switch strategy using supervisory centralized MPC can reduce calculation time compared to the decentralized MPC, so the settling time is slightly less, about 2100 seconds, and there is a similar temperature error.

V. CONCLUSION

The proposed supervisor model-switch strategy employs the system identification method and supervisory centralized MPC to control each room's temperature and to maintain positive superheat in the one-to-many VRF system, thereby addressing the room temperature coupling problem. The single-input, single-output linearized models are pre-established using the compressor speed and the indoor unit's electronic expansion valves as inputs, and the room temperature and corresponding superheat temperature as outputs. The first-order linear models represent the one-to-three VRF system with equilibrium room temperatures of 26.5°C, 25°C, and 23.5°C. The supervisor in the flowchart determines whether there is a steady-state input between the equilibrium temperature and the user-set temperature for all models, then calculates the MDT from the current model to another, which utilizes switching the appropriate model as a reference model for MPC.

The supervisor model-switch strategy has been verified by simulating the proper superheat weights in MPC; the approach has been numerically validated by controlling room temperatures from 26.5°C through 25°C to 23.5°C. The one-to-three VRF system experiments were conducted with and without a supervisor to verify the stability of the supervisor model-switch strategy. For MPC alone applied in the experiment, with the VRF system controlling room temperature from 28.3°C to 26°C, a steady-state error of less than 0.5°C was achieved even after the oil return condition. In the second experiment in which the supervisor model-switch strategy was employed, with varying initial room temperatures of 31°C, 29°C, and 28°C corresponding to distinct thermal loads, the user-set temperatures were changed with the executed time series. The room temperature results revealed that model switching was automatically regulated six times across the three models. This control approach effectively guided the room temperatures to reach the desired temperatures of 26°C, 25°C, and 24°C within 0.5°C. The results indicate that the supervisor model-switch strategy can effectively maintain the user-set temperature, expand the controllable area, and demonstrate the potential for many-to-many VRF system control.

REFERENCES

[1] X.-D. He, S. Liu, H. H. Asada, and H. Itoh, "Multivariable control of vapor compression systems," *HVAC&R Res.*, vol. 4, no. 3, pp. 205–230, Jul. 1998.

[2] J.-L. Lin and T.-J. Yeh, "Modeling, identification and control of air-condition systems," *Int. J. Refrig.*, vol. 30, pp. 209–220, Dec. 2007.

[3] J.-L. Lin and T.-J. Yeh, "Identification and control of multi-evaporator air-conditioning system," *Int. J. Refrig.*, vol. 30, pp. 1374–1385, Dec. 2007.

[4] D. M. K. K. V. Rao and A. Ukil, "Modeling of room temperature dynamics for efficient building energy management," *IEEE Trans. Syst., Man, Cybern., Syst.*, vol. 50, no. 2, pp. 717–725, Feb. 2020.

[5] Z. Jun and Z. Kanyu, "A particle swarm optimization approach for optimal design of PID controller for temperature control in HVAC," in *Proc. 3rd Int. Conf. Measuring Technol. Mechatronics Autom.*, vol. 1, Jan. 2011, pp. 230–233.

[6] H. Moradi, M. Saffar-Avval, and F. Bakhtiari-Nejad, "Nonlinear multivariable control and performance analysis of an air-handling unit," *Energy Buildings*, vol. 43, no. 4, pp. 805–813, Apr. 2011.

[7] G. D. Pasgianos, K. G. Arvanitis, P. Polycarpou, and N. Sigrimis, "A nonlinear feedback technique for greenhouse environmental control," *Comput. Electron. Agricult.*, vol. 40, nos. 1–3, pp. 153–177, Oct. 2003.

[8] M. Anderson, M. Buehner, P. Young, D. Hittle, C. Anderson, J. Tu, and D. Hodgson, "MIMO robust control for HVAC systems," *IEEE Trans. Control Syst. Technol.*, vol. 16, no. 3, pp. 475–483, May 2008.

[9] M. M. Gouda, S. Danaher, and C. P. Underwood, "Thermal comfort based fuzzy logic controller," *Building Services Eng. Res. Technol.*, vol. 22, no. 4, pp. 237–253, Nov. 2001.

[10] J. Liang and R. Du, "Thermal comfort control based on neural network for HVAC application," in *Proc. IEEE Conf. Control Appl.*, Toronto, ON, Canada, Aug. 2005, pp. 819–824.

[11] H. A. Dyvia and C. Arif, "Analysis of thermal comfort with predicted mean vote (PMV) index using artificial neural network," *IOP Conf. Ser., Earth Environ. Sci.*, vol. 622, Nov. 2021, Art. no. 012019.

[12] C. E. Garcáa, D. M. Prett, and M. Morari, "Model predictive control: Theory and practice—A survey," *Automatica*, vol. 25, no. 3, pp. 335–348, May 1989.

[13] A. Afram and F. Janabi-Sharif, "Theory and applications of HVAC control systems—A review of model," *Building Environ.*, vol. 72, pp. 343–355, Feb. 2014.

[14] X.-C. Xi, A.-N. Poo, and S.-K. Chou, "Support vector regression model predictive control on a HVAC plant," *Control Eng. Pract.*, vol. 15, no. 8, pp. 897–908, Aug. 2007.

[15] P.-D. Moroşan, R. Bourdais, D. Dumur, and J. Buisson, "Building temperature regulation using a distributed model predictive control," *Energy Buildings*, vol. 42, no. 9, pp. 1445–1452, Sep. 2010.

[16] X. Xu, S. Wang, and G. Huang, "Robust MPC for temperature control of air-conditioning systems concerning on constraints and multitype uncertainties," *Building Services Eng. Res. Technol.*, vol. 31, no. 1, pp. 39–55, Jan. 2010.

[17] G. Huang, S. Wang, and X. Xu, "A robust model predictive control strategy for improving the control performance of air-conditioning systems," *Energy Convers. Manage.*, vol. 50, no. 10, pp. 2650–2658, Oct. 2009.

[18] W. Yang, G. Feng, and T. Zhang, "Robust model predictive control for discrete-time Takagi–Sugeno fuzzy systems with structured uncertainties and persistent disturbances," *IEEE Trans. Fuzzy Syst.*, vol. 22, no. 5, pp. 1213–1228, Oct. 2014.

[19] L. Teng, Y. Wang, W. Cai, and H. Li, "Robust model predictive control of discrete nonlinear systems with time delays and disturbances via T–S fuzzy approach," *J. Process Control*, vol. 53, pp. 70–79, May 2017.

[20] C. Anuntasethakul and D. Banjerdpongchai, "Design of supervisory model predictive control for building HVAC system with consideration of peak-load shaving and thermal comfort," *IEEE Access*, vol. 9, pp. 41066–41081, 2021.

[21] M. S. Elliott and B. P. Rasmussen, "Decentralized model predictive control of a multi-evaporator air conditioning system," *Control Eng. Pract.*, vol. 21, no. 12, pp. 1665–1677, Dec. 2013.

[22] N. Jain, D. J. Burns, S. Di Cairano, C. R. Laughman, and S. A. Bortoff, "Model predictive control of vapor compression systems," in *Proc. 15th Int. Refrig. Air Cond. Conf.*, Jul. 2014, pp. 1–11.

[23] P. Mhaskar, N. H. El-Farra, and P. D. Christofides, "Predictive control of switched nonlinear systems with scheduled mode transitions," *IEEE Trans. Autom. Control*, vol. 50, no. 11, pp. 1670–1680, Nov. 2005.

[24] M. Pasamontes, J. D. Álvarez, J. L. Guzmán, J. M. Lemos, and M. Berenguel, "A switching control strategy applied to a solar collector field," *Control Eng. Pract.*, vol. 19, no. 2, pp. 135–145, Feb. 2011.

[25] B. A. H. Vicente and P. A. Trodden, "Switching tube-based MPC: Characterization of minimum dwell-time for feasible and robustly stable switching," *IEEE Trans. Autom. Control*, vol. 64, no. 10, pp. 4345–4352, Oct. 2019.

[26] G. Chesi, P. Colaneri, J. C. Geromel, R. Middleton, and R. Shorten, "A nonconservative LMI condition for stability of switched systems with guaranteed dwell time," *IEEE Trans. Autom. Control*, vol. 57, no. 5, pp. 1297–1302, May 2012.
[27] M. Kumar, I. N. Kar, and A. Ray, "State space based modeling and performance evaluation of an air-conditioning system," *HVAC&R Res.*, vol. 14, no. 5, pp. 797–816, Sep. 2008.
[28] D. Wang, M. Li, M. Guo, Q. Shi, C. Zheng, D. Li, S. Li, and Z. Wang, "Modelling variable refrigerant flow system for control purpose," *Energy Buildings*, vol. 292, Aug. 2023, Art. no. 113163.
[29] L. Zhang, S. Zhuang, and R. D. Braatz, "Switched model predictive control of switched linear systems: Feasibility, stability and robustness," *Automatica*, vol. 67, pp. 8–21, May 2016.

CHUN-YEON LIN (Member, IEEE) received the B.S. degree in mechanical engineering from National Central University, Taoyuan, Taiwan, in 2003, the M.S. degree in electrical control engineering from National Chiao Tung University, Hsinchu, Taiwan, in 2005, the M.S. degree in mechanical engineering from Stanford University, Stanford, CA, USA, in 2011, and the Ph.D. degree in mechanical engineering from Georgia Institute of Technology, Atlanta, GA, USA, in 2017. He is currently an Associate Professor with the Department of Mechanical Engineering, National Taiwan University, Taipei, Taiwan. His current research interests include mechatronics, sensing systems, robotics, and system dynamics and control.

TING-KUAN LIAO received the B.S. degree in mechanical engineering from National Chung Hsing University, Taichung, Taiwan, in 2021, and the M.S. degree in mechanical engineering from National Taiwan University, Taipei, Taiwan, in 2023. He is currently a Research and Development Engineer with Delta Electronics, Inc. His research interests include model predictive control, variable refrigerant flow systems, and switch control.

HSIN-HAO CHOU received the B.S. degree in mechanical engineering from the National Taipei University of Technology, Taipei, Taiwan, in 2022. He is currently pursuing the M.S. degree in mechanical engineering, National Taiwan University, Taipei. His research interests include model predictive control, variable refrigerant flow systems, and embedded systems.

YI-CHIN WU (Member, IEEE) received the B.S. degree in mechanical engineering from National Cheng Kung University, Tainan, Taiwan, in 2019, and the M.S. degree in mechanical engineering from National Taiwan University, Taipei, Taiwan, in 2021, where he is currently pursuing the Ph.D. degree. His research interests include mechatronics and electromagnetic systems.

CHIEN-CHANG WANG received the B.S. and M.S. degrees in physics from the Soochow University, National Chung Cheng Universities, Taiwan, in 1995 and 1997, respectively, and the Ph.D. degree in material and science and engineering from National Chiao Tung University, Taiwan, in 2008. From 1999 to 2003, he was an Associate Engineer with the Optical Electronical System Laboratory, ITRI. From 2003 to 2012, he was an Engineer with the Green Energy and Environment Research Laboratories (GEL), ITRI. Since 2012, he has been a Senior Engineer with the GEL. Currently, he is the Management of Mechatronics Key-Modules Department of the GEL. His research interests include magnetic circuit design, micro motors, high-power and high-speed electric machines and applications, compressors, vibration and noise diagnostics, heating and refrigeration applications.

SHY-HER NIAN received the M.S. degree in refrigerating air-conditioning engineering from the National Taipei University of Technology, Taipei, Taiwan, in 2003. After two years of military service, he joined the Industrial Technology Research Institute, in 2005. His research interests include the design of air condition systems and heat pump systems, experiments design, and performance testing.

MENG-YEN TSAI received the M.S. and Ph.D. degrees in mechanical engineering from National Chiao Tung University, Hsinchu, Taiwan, in 2005 and 2010, respectively. He has been with the Green Energy and Environmental Laboratory, Industrial Technology Research Institute, Hsinchu, since 2011.

TSAI-WANG HUNG received the M.S. degree in electrical engineering from Tatung Institute of Technology, in 1990. After working for a year with Tatung Company, he joined the Industrial Technology Research Institute, in 1995. His research interests include the design of control algorithms, saving power control, and system control.